Meccanica
DOI 10.1007/s11012-014-9924-y

Transient dynamic response of debonded sandwich plates predicted with finite element analysis

Vyacheslav N. Burlayenko · Tomasz Sadowski

Received: 28 August 2013 / Accepted: 8 March 2014

Abstract Dynamic transient response of a composite sandwich plate with a penny-shaped debonded zone has been studied by using the finite element analysis within the ABAQUS/Explicit code in this paper. In order to accurately predict the response of the debonded sandwich plate to impulsive loading, contact–impact and sliding conditions along the damaged skin-to-core interface were imposed in the model through a kinematic predictor/corrector contact algorithm. The accuracy of the finite element (FE) model used was verified by comparing between numerical predictions and experimental data known in literature for the frequency spectrum of a cracked polycarbonate laminated beam containing a delamination. By analyzing nonlinear aspects of the transient dynamics of the sandwich plate, it is shown that the presence of the debond significantly alters its short-term response. In this respect, a considerable influence of contact events within the debonded region on the plate's global dynamic response was found out. These results were presented in both time and frequency domains. The predictions performed also showed that the FE model applied would be useful for nondestructive evaluation of defects in composite sandwich plates, and for studying dynamic response of such plates to impact.

Keywords Sandwich plates · Skin-to-core debond · Nonlinear transient vibrations · Dynamic contact · Finite element analysis

V. N. Burlayenko (✉)
Department of Applied Mathematics, National Technical University 'KhPI', Frunze, 21, Kharkiv 61002, Ukraine
e-mail: burlayenko@yahoo.com

T. Sadowski
Department of Solid Mechanics, Lublin University of Technology, Nadbystrzycka, 40, 20-618 Lublin, Poland
e-mail: t.sadowski@pollub.pl

1 Introduction

Composite sandwich materials are referred to structural materials whose properties might be tailored for creating high performance structures [1]. This their ability makes such materials more attractive over the traditional ones for using in different engineering applications. However, because sandwich materials consist technologically of high distinctive constituent layers, they exhibit a more sensitivity to damage. One of the most frequently concerns encountered in composite sandwich materials is interfacial cracking or the loss of cohesion between the basic layers, known as skin-to-core debonding. The presence of debond within a sandwich structure is known to cause reduction of overall stiffness and strength, to alter vibrational characteristics and may even lead to its eventual disintegration [2]. Therefore, a study of debonding effects on the mechanical behavior of sandwich structures is of importance.

Published online: 25 March 2014

Due to the wide practical applications of sandwich plate-like structures in aircrafts, automotive vehicles and marine shipping industry, dynamics of sandwich plates is a subject of intensive investigations in this respect. A considerable amount of research efforts pertains to prediction of natural frequencies and appropriate mode shapes of debonded sandwich plates. Most of analytical and numerical models developed to describe this issue are based on linear approaches in which contact between the segments detached at the skin-to-core interface is neglected. It is usually assumed that the debonded parts are either freely penetrating to each other or constrained to move together or separated by additional spring elements, see e.g. [3–7] among of others. Effects of multiple debonding on free oscillations of sandwich plates have been studied using the similar models in [8, 9]. The modified Galerkin method was used to solve a free vibration problem, formulated for a simply supported debonded sandwich beam with a rectangular cross-section, by using the Hamilton's variational principle along with the high-order sandwich panel theory in [10].

Another a common feature of those practical applications is a dynamic transient behavior of sandwich panels. Low velocity impacts, air blast and underwater blast loads, by which aircrafts, marine and automotive vehicles are exposed during in-service life are examples of suddenly applied loads resulting in short-term transient oscillations in their sandwich structural components. The understanding of transient failure modes is vital for structural durability and damage tolerance of sandwich panels, e.g. [11, 12]. The transient dynamic response of sandwich panels containing a post-damaged partial debond at the layered interface allows one to evaluate their residual structural performance. In addition, in context of structural health monitoring, some vibration-based nondestructive evaluations of defects in damaged structures including a debond within sandwich panels rely on transient data, e.g. [13, 14]. The accurate prediction of real time transient dynamic response in debonded sandwich panels is possible, when intermittent contact between skin and core in the damaged interface can be modelled in detail. Hence, nonlinear analysis is required to be applied to such problems. As a result, numerical difficulties arise of contact modelling that makes the use of pure analytical models restricted in the aforementioned investigations, while numerical approaches are widely utilized for that.

Because of versatility in solving complex topological and multi-physical problems, the finite element method (FEM) has been used by many researchers for studying dynamics of laminated and sandwich plates accounting for intermittent contact within the damaged interface. In [15] intermittent contact between delaminated segments of a composite beam has been modeled using a node-to-node frictionless contact formulation. The contact constraints were imposed by a modified Lagrange multiplier method. An implicit Newmark algorithm was exploited for time-stepping procedure to predict dynamic response of the delaminated beam under both impulse and harmonic loads. Authors in [16] investigated transient dynamics of a debonded sandwich beam using a finite element (FE) model, where time dependent contact conditions at the damaged interface were simulated with a kinematic node-to-node frictionless contact algorithm. The transient analysis of delaminated smart composite plates has been studied in [17] using an improved layerwise laminate theory. Both large deformations and interlaminar contact within the delaminated zone were taken into account. The "breathing" phenomenon of delamination was simulated by applying two distinctive contact spring models. The associated governing equations were integrated with a modified predictor–corrector method involving the Newmark-beta algorithm and Newton–Raphson iterations. A much more sophisticated FE beam model in respect of contact–impact between a thin detached part and a remaining part of beam has been formulated in [18]. Authors applied the surface-to-surface frictionless contact algorithm within the penalty method within the LS-DYNA code. The penalty parameter and the contact damping value were varied to fit experiment data obtained by the authors previously. A nonlinear dynamic analysis of sandwich plates containing a post-impact zone involving core fracture and interfacial debond under impulse and harmonic loads has been performed in [19]. In those simulations to model the contact phenomenon during forced oscillations, the surface-to-surface contact definition and kinematic contact algorithm within the ABAQUS/Explicit code were used. Although in that paper the global dynamic response of the sandwich plates was examined, however, the contact phenomenon existing between the detached skin and core was not investigated in detail. A rigorous mathematical formulation based on the formalism of continuum mechanics for the underlying elastodynamic problem of a body with an interfacial

crack involving the Signorini's and Coulomb's laws and a finite element statement of the problem within an explicit scheme were presented in [20]. Finite element simulations with the ABAQUS/Explicit code of transient response and forced dynamics of a simply supported rectangular sandwich plate with a penny-shaped debonded zone were considered as examples of applying that FE modeling. While the research provided the nonlinear dynamic analysis of debonded sandwich plates accounting for contact, the performed numerical studies examined only global dynamics and no detailed features of nonlinearity sources caused by intermittent contact arising within the debonded zone were analyzed. However, the knowledge about that local dynamic process could shed light on the more understanding of the debonded plates' dynamic problem itself.

In the present paper we aim to investigate the influence of intermittent contact between the detached skin and core on the global transient response of a sandwich plate containing skin-to-core debond. Using the three-dimensional FE model of the sandwich plate developed in [20], the transient dynamic behavior of a simply supported rectangular sandwich plate with a central penny-shaped debonded zone is studied in the current work. Comparisons between transient responses of the debonded sandwich plate and the same intact plate, obtained with the ABAQUS/Explicit code are used to make conclusions about the influence of intermittent contact on the sandwich plate's short-time dynamics. Time histories and frequency spectrum contents of signals acquired from the both sandwich plates are compared and analyzed for this purpose. Studies for different sizes of the debonded zone are carried out to clarify the dissipative character of intermittent contacts and to emphasize their influence on the dynamics and dynamic stress state of the debonded sandwich plate. The detailed analysis of contact–impact events in the debonded zone is performed for discovering effects invoked by nonlinear contact–friction interactions and, as a result, to gain the better understanding of the transient dynamic behavior of sandwich plates with interface defects.

2 Finite element modeling

Let us consider a rectangular sandwich plate containing a penny-shaped zone of radius R detached at the center between the upper skin and the core, as shown in Fig. 1. The dynamics of the debonded sandwich plate is inherently nonlinear even for the presumed case of small displacement kinematics and the simplest linear constitutive relations because the contact area between the detached skin and core is a priori unknown and additional boundary conditions or constraints on the relative displacements and traction in the debonded zone should be imposed. Thereby, the elastodynamic problem formulated for the debonded sandwich plate involves a complete set of equations relating to the initial boundary-value problem with boundary conditions being a part of the solution. To get a solution, approaches based on numerical procedures discretising the problem are commonly utilized. In this context, the FEM is the most used modelling technique. Finite element formulations of elastodynamic problems with contact as well as some numerical solutions for cracked bodies accounting for contact between crack surfaces can be found in books on contact mechanics, e.g. [21, 22] and recent papers, e.g. [23, 24], respectively. Here, only a general finite element approximation of the problem at hand is briefly presented below.

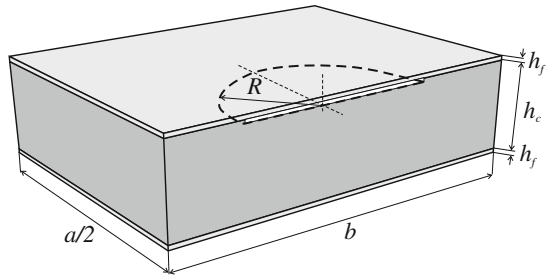

Fig. 1 Half of sandwich plate with penny-shaped debonded zone

2.1 Finite element equations of motion with contact

Following the standard displacement-based finite element statement of the elastodynamic problem with contact and friction, displacements between contacting surfaces should be constrained by impenetrability conditions, i.e. none of material points is allowed to be penetrated. Besides, the displacement field being applied should be able to describe the discontinuous behavior introduced by friction, i.e. sticking and sliding situations as well as to trace a path as a result of sliding. In respect to kinetic requirements, contact

traction arising due to normal contact should be not tensile, and frictional contact forces have to oppose sliding directions. Also, the balance of momentum on a contact boundary should be fulfilled.

A general form of the finite element solution of the aforementioned problem with assumptions of linear elasticity and small deformations can be written as the following set of nonlinear differential equations:

$$\mathrm{M}\ddot{\mathrm{U}}(t) + \mathrm{C}\dot{\mathrm{U}}(t) + \mathrm{K}\mathrm{U}(t) = \mathrm{F}^{ext}(\mathrm{U}(t)) - \mathrm{F}^{cont}(\mathrm{U}(t)) \tag{1}$$

Herewith the system (1) should be subjected to initial conditions on $\dot{\mathrm{U}}(0)$ and $\mathrm{U}(0)$, boundary conditions on a predefined surface, and impenetrability and friction conditions on a boundary associated with contacting surfaces.

In (1) at each instant of time t we define that $\ddot{\mathrm{U}}(t)$, $\dot{\mathrm{U}}(t)$ and $\mathrm{U}(t)$ are the global vectors of unknown accelerations, velocities and displacements, F^{ext} and F^{cont} are the global vectors of the given external and calculated contact forces, and M, C and K are the global mass, damping and stiffness matrices, respectively. These global vectors and matrices are typically calculated by the assembly of element level contributions [25].

It should be noted that the vector of contact forces F^{cont} consists of normal and tangential elements, which are defined by appropriate normal t_N and tangential t_T components of a contact traction vector $\mathrm{t}_c = \mathrm{t}_N + \mathrm{t}_T$ for each contact pair. In turn the contact pressure components are conjugated to normal g_N and tangential g_T gap functions describing the relative movements of contacting surfaces with respect to each other in the normal and tangential directions, respectively. In terms of the "master–slave" contact definition commonly used in the finite element formulation, the gap functions can be presented in the forms [22]:

$$g_N = (\mathrm{x}^- - \bar{\mathrm{x}}^+) \cdot \bar{\mathrm{n}}^+ \tag{2}$$

and

$$\mathrm{g}_T = g_{T_\alpha} \bar{\mathrm{a}}^{+^\alpha} \text{ with } g_{T_\alpha} = (\mathrm{x}^- - \bar{\mathrm{x}}^+) \cdot \bar{\mathrm{a}}_\alpha^+, \tag{3}$$

where x^- is a point of slave surface and $\bar{\mathrm{x}}^+(\bar{\xi}^1, \bar{\xi}^2)$ is its orthogonal projection on the master surface parameterized by ξ^α $(\alpha = 1, 2)$, and $\bar{\mathrm{n}}^+$ is the unit vector normal to the master surface and $\bar{\mathrm{a}}_\alpha$ $(\alpha = 1, 2)$ are the tangent base vectors at the point $\bar{\mathrm{x}}^+$. In the geometrically linear case, the rate of tangential gap function at this point can be found as

$$\dot{\mathrm{g}}_T = \dot{\bar{\xi}}^\alpha \bar{\mathrm{a}}_\alpha^+ = \dot{g}_{T_\alpha} \bar{\mathrm{a}}^{+^\alpha} \text{ with } \dot{g}_{T_\alpha} = \left(\dot{\mathrm{x}}^- - \dot{\bar{\mathrm{x}}}^+\right) \cdot \bar{\mathrm{a}}_\alpha^+ = a_{\alpha\beta} \dot{\bar{\xi}}^\beta, \tag{4}$$

where $a_{\alpha\beta} = \bar{\mathrm{a}}_\alpha^+ \cdot \bar{\mathrm{a}}_\beta^+$ is the metric tensor at $\bar{\mathrm{x}}^+$.

Then the impenetrability conditions known as Karush–Kuhn–Tucker inequalities can be formulated as follows:

$$t_N \le 0,\ g_N \ge 0 \text{ and } t_N g_N = 0, \tag{5}$$

where t_N is the scalar quantity of the normal contact pressure, i.e. $\mathrm{t}_N = t_N \bar{\mathrm{n}}^+$.

The friction conditions arising in tangential directions can be written in the form:

$$\|\mathrm{t}_T\| \le \tau_{crit},\ \|\mathrm{g}_T\| \ge 0,\ (\|\mathrm{t}_T\| - \tau_{crit})\|\mathrm{g}_T\| = 0, \tag{6}$$

where τ_{crit} is a threshold of tangential contact traction when a tangential slip occurs. The value of threshold is evaluated according with a friction law adopted. The Coulomb friction law defines $\tau_{crit} = \mu t_N$, where μ is the coefficient of friction.

The using an analogy between plasticity and friction leads to the following form of (6):

$$\dot{\mathrm{g}}_T^{slip} = \dot{\gamma} \frac{\partial \Phi(\mathrm{t}_T)}{\partial \mathrm{t}_T} = \dot{\gamma} \frac{\mathrm{t}_T}{\|\mathrm{t}_T\|}, \tag{7}$$

along with loading–unloading conditions in the form:

$$\Phi \le 0,\ \dot{\gamma} \ge 0 \text{ and } \Phi\dot{\gamma} = 0, \tag{8}$$

where $\dot{\gamma}$ is the slip rate parameter and the potential function is presented as $\Phi(\mathrm{t}_T) = \|\mathrm{t}_T\| - \mu t_N$.

In (1) the system material damping defined by the matrix C is assumed that can be represented by Rayleigh damping [26]:

$$\mathrm{C} = \alpha \mathrm{M} + \beta \mathrm{K} \tag{9}$$

The factors α and β can be determined on the basis of the modal damping ratio as follows:

$$\xi_n = \frac{\alpha}{2\omega_n} + \frac{\beta\omega_n}{2}, \tag{10}$$

by specifying any desirable ratio for any two selected frequencies ω_n of the undamped system with the given M and K.

2.2 Explicit time-stepping procedure

The semi-discrete system of equations (1) has to be completely discretized in a time domain. For this the time interval $[0,T]$ is divided into non-overlapping subintervals such that $[0,T]=\bigcup_{i=0}^{L-1}[t_i,t_{i+1}]$, where $t_i<t_{i+1}$, and $t_0=0$, $t_L=T$. Hence, the solution satisfying (1) can only be found in a finite number of time steps. Let the time increment be $\triangle t_{i+1}=t_{i+1}-t_i$ and for the simplicity accelerations, velocities and displacements referring to this time increment are denoted by $\ddot{\mathrm{U}}_{i+1}$, $\dot{\mathrm{U}}_{i+1}$ and U_{i+1}, respectively. Then the totally discretized system of equations (1) at a certain instant of time $t_{i+1}=t_i+\triangle t_{i+1}$ can be written down as follows:

$$\mathrm{M}\ddot{\mathrm{U}}_{i+1}+\mathrm{C}\dot{\mathrm{U}}_{i+1}+\mathrm{K}\mathrm{U}_{i+1}=\mathrm{F}_{i+1}^{ext}-\mathrm{F}_{i+1}^{cont}, \tag{11}$$

with the initial conditions $\mathrm{U}_0=\bar{\mathrm{U}}$ and $\dot{\mathrm{U}}_0=\bar{\mathrm{V}}$, given boundary conditions and boundary conditions being calculated due to developing contact.

Following the explicit time-stepping algorithm based on the central difference operator (see e.g. [25]), first, accelerations at the beginning of each increment $\triangle t_{i+1}$ are calculated. For this purpose the Eq. (11) is reexpressed in the form:

$$\ddot{\mathrm{U}}_i=\mathrm{M}^{-1}(\mathrm{F}_i^{ext}-\mathrm{F}_i), \tag{12}$$

where F_i^{ext} is the vector of the given external nodal forces at time t_i and F_i is the sum of nodal internal $\mathrm{F}_i^{int}=\mathrm{K}\mathrm{U}_i$, damping $\mathrm{F}_i^{damp}=\mathrm{C}\dot{\mathrm{U}}_i$ and contact F_i^{cont} forces which are updated during the previous time increment $\triangle t_i$.

Thereafter, the accelerations calculated at t_i are used to advance the velocity solution to $t_i+\frac{1}{2}\triangle t_{i+1}$ and the displacement solution to $t_i+\triangle t_{i+1}$ in accordance with the following formulas:

$$\begin{aligned}\dot{\mathrm{U}}_{i+\frac{1}{2}}&=\dot{\mathrm{U}}_{i-\frac{1}{2}}+\frac{\triangle t_{i+1}+\triangle t_i}{2}\ddot{\mathrm{U}}_i\\ \mathrm{U}_{i+1}&=\mathrm{U}_i+\triangle t_{i+1}\dot{\mathrm{U}}_{i+\frac{1}{2}}\end{aligned} \tag{13}$$

The initial half-step lagging of velocity $(\dot{\mathrm{U}}_{-1/2})$ is calculated from the initial velocity assuming that the initial acceleration is constant over the lagging half-step.

The key to the computational efficiency of the explicit procedure is the use of a diagonal (or lumped) mass matrix, i.e. the mass matrix M is being understood as lumped in (11). Then, the inversion of the mass matrix that is employed in the computation for the accelerations in (12) is computationally very fast. As resulted from (11)–(13), the explicit algorithm advances the kinematic state known from a previous increment to the next one without iterations and tangent stiffness matrix and, thus, no equations are being solved simultaneously that saves the computational time significantly. Moreover, the computational cost in the explicit integration procedure rises linearly with problem size. However, the explicit time integration is only conditionally stable, i.e. the time increment used for integrating over time in (11) must be smaller than the stability limit of the central-difference operator, [25]. An estimation of this limit is the transit time of a dilatational wave speed (c_d) across the length of the smallest element in a finite element mesh (L_e), i.e.

$$\triangle t_{crit}\approx\frac{L_e}{c_d} \tag{14}$$

2.3 Kinematic contact algorithm

An explicit form of expressions applied to compute the contact forces F_{i+1}^{cont} in (11) at each time increment is defined by a contact algorithm used. In this work the kinematic contact algorithm is suggested to be employed. It is a predictor/corrector method enabling to impose exactly the constraints (5), and (7) and (8) on the global equations (11) by modifying accelerations, velocities and displacements of nodes, at which contact is active in the current time increment. An algorithmic setting of the kinematic contact approach within the explicit time integration scheme can be found in [20]. A short description of this algorithm is given below.

In the predictor phase, a kinematic state of the model in the time increment Δt_{i+1} is advanced by ignoring any contact conditions. This may result in penetration and overpredicted slip, as shown by the configuration of a slave node S in Fig. 2.

Then, the contact force $f_{N_S}^{cont}$ resisting to penetration is calculated as a function of penetration depth $(d_N)^{pred}$ of the slave node, its mass m_S and time increment Δt_{i+1}. Analogously, the unconstrained rate of tangential movement $(v_{T\alpha})^{pred}$ of the slave node with respect to the master surface in the direction α, the node mass and the time increment are used to calculate a

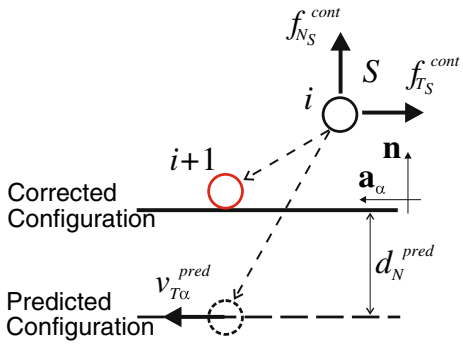

Fig. 2 Kinematic contact constraint algorithm

tangential contact force $f_{T_S}^{pred}$ required to oppose sliding. In the corrector phase of this time increment, for each such slave node contacting with or penetrating through the master surface, an acceleration correction is applied to recover its predicted penetration and/or sliding as follows [27]:

$$\ddot{\mathrm{U}}_S^{corr} = \ddot{\mathrm{U}}_S^{pred} + \ddot{\mathrm{U}}_{N_S} + \ddot{\mathrm{U}}_{T_S}, \tag{15}$$

where $\ddot{\mathrm{U}}_S^{pred}$ is the predicted acceleration of the slave node, $\ddot{\mathrm{U}}_{N_S}$ and $\ddot{\mathrm{U}}_{T_S}$ are acceleration corrections reflecting the response of the master surface to the contact forces $f_{N_S}^{cont}$ and $f_{T_S}^{cont}$, respectively. From those corrected accelerations, the velocities at $\triangle t_{i+1/2}$ and the displacements at $\triangle t_{i+1}$, i.e. at a final configuration in which the slave nodes are exactly in compliance with the master surface can be found solving (13). Therefore, the vector of contact force F_{i+1}^{cont} including both the normal and tangential components is determined as well as the updated configuration specified by the displacement vector U_{i+1} is found.

It is worth to be noted that to apply a certain contact algorithm at each time increment for calculating the contact forces F_{i+1}^{cont}, a set of active contact constraints should be known before solving (11). The active set of constraints is defined by an iterative process called as contact searching. This algorithm involves two phases: the global search that locates the closest to each other segments, and the local search that calculates the gap functions g_N^h and g_T^h on the contact boundary between the segments found in the global search. For more details on search algorithms we refer to books on contact mechanics, e.g. [21, 22].

2.4 Finite element model

The FE model used for a simply supported rectangular sandwich plate with a circular debonded zone at the center of the skin-to-core interface is the same model that was developed in [20]. For the sake of completeness, that model is briefly presented here.

In Fig. 3a the FE model of the debonded sandwich plate developed with the ABAQUS code is shown. Reduced integrated 8-node continuum shell finite elements SC8R with displacement degrees of freedom only are used for discretization of the skins. These elements enable to model both thin and thick plate/shell problems. In the case of skins made of laminated composites, the continuum shell elements are stacked to provide a more refined through-the-thickness response.The core of the sandwich plate is modelled with first-order reduced integrated 8-node continuum solid "brick" elements C3D8R which are directly connected to nodes of the continuum shell elements representing the skins. To avoid the hour-glassing

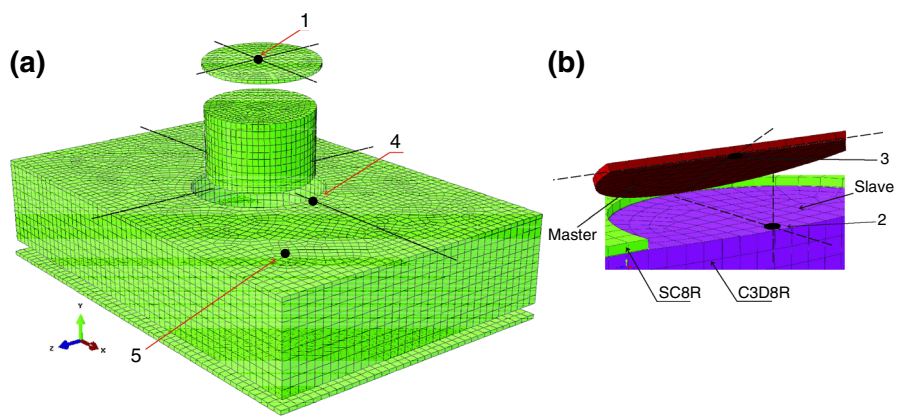

Fig. 3 The debonded sandwich plate with penny-shaped debonded zone: **a** three-dimensional FE model; and **b** details of modeling at the debonded zone

problem in these elements, the "hourglass stiffness" method available in ABAQUS is used. Moreover, the improved "centroidal strain" formulation in computation of strains at the elements is utilized to increase the efficiency of the ABAQUS/Explicit solver. More details concerning the finite elements involved can be found in [28].

The complicated mesh geometry of the debonded sandwich plate is generated by partition of the total FE model onto several parts, which are connected with each other through the share nodes. The penny-shaped debonded zone is presented by an actual small gap between the finite elements of the upper skin and the core. The mesh density is higher in the central part of the plate, where the contact–impact phenomenon is expected to be modelled and it is rougher for the remaining part of the plate. No artificial adjustment of either the material or geometrical properties is made at the debonded region to ensure as close as possible a physically real case.

The surface-to-surface contact model in the Explicit version of ABAQUS is utilized for the detached parts in the skin-to-core interface. Contact pairs between those surfaces that may come into contact with each other during the analysis are formed by faces of the appropriate underlying finite elements. Since the surfaces coming into contact have high dissimilar mechanical properties, a pure master–slave contact pair formulation is used, Fig. 3b. Because surface-to-surface contact is applied, meshes of two contacting surfaces should not be perfectly matched to each other. Moreover, this type of contact implies that contact conditions are enforced in an average sense over regions nearby slave nodes rather than only at an individual slave node. Thereby, it provides more accurate contact stress and pressure results [28]. The small-sliding contact tracking algorithm is utilized for the contacting surfaces because small oscillations are presumed. The "hard" contact model available in the FE code implying no penetration at each constraint location and no contact pressure transmission unless the surfaces are in contact is accepted to model normal interactions between the contacting surfaces. The isotropic Coulomb friction model specifies the contact behavior of these surfaces in tangential directions. The contact constraints are imposed and the contact forces are calculated by using the kinematic contact enforcement method described shortly in Sect. 2.3.

To realize the boundary conditions of simply supported edges, all vertical and one of in-plane displacements of the skins' finite elements depending on the edge location within the coordinate system are constrained. It is assumed that initial displacements and velocities are zero, i.e. the transient motion begins from the sandwich plate at rest. An impulse load is applied as a concentrated force acting as a step function at a certain node of the FE model, i.e.

$$F(t) = \begin{cases} F_0, & 0 \le t \le t_* \\ 0, & t > t_* \end{cases}$$

The duration of the applied force t_* was taken much shorter than the analysis time t_{end} (one tenth of the analysis time).

3 Numerical results

3.1 Beam finite element model

First, the performance of the FE model, described in the preceding section and the fidelity of nonlinear transient dynamic simulations performed with this model were verified to correctly deal with these problems. Because results of transient response for a debonded sandwich plate was not found in the literature, the transient dynamic analysis of a delaminated polycarbonate three-layer composite beam containing also a transverse crack, for which experimental results are known in [29], is carried out. It should be noted that although the beam example does not include all issues stemming from distinct materials in different layers, as it takes place for a sandwich plate, convergence studies within the explicit marching scheme and results treatment based on the signal processing technique are the same as for the plate model.

The beam was clamped on one end and loaded by an instant force on the other end with $t_* = 10$ ms and $F_0 = 5$ N. In this case the step load was simulated as described in the test. The dimensions of the delaminated beam, the same as in [29] are 610 mm long by 51 mm wide and by 12.1 mm thick. The crack is located 249 mm from the clamped end and the delaminated region splitting the first and second constitutive layers by the gap of 0.2 mm is extended 30 mm towards the clamped end and 48 mm towards the free end. The beam is constructed with the layers of

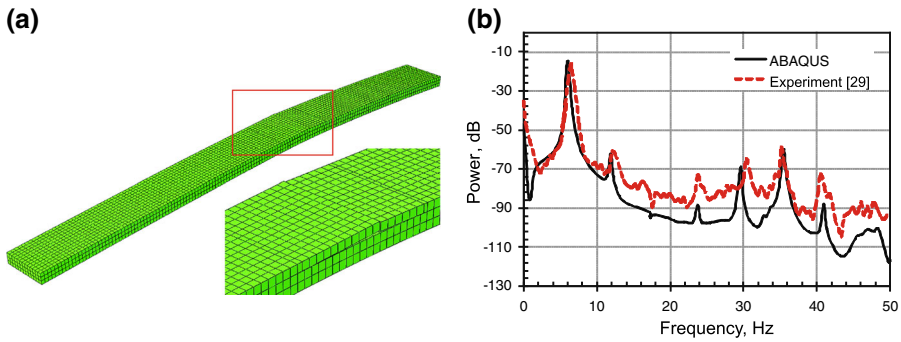

Fig. 4 The FE model of the delaminated beam: **a** the deformed shape; and **b** the power spectrum at the point of free end

equal thickness. Mechanical properties of the polycarbonate material are accepted as the following: Young's modulus is 2,400 MPa, Poisson's ratio is 0.37, material density is 1,200 kg m^{-3} and coefficient of friction is 0.38.

The FE model of sandwich plate presented in Fig. 3a was appropriately modified into a three-dimensional delaminated beam model, as shown in Fig. 4a. The three dimensional continuum finite elements C3D8R [28] were used for meshing the beam. The mesh contained the 6,000 finite elements with aspect ratio near one and, herewith, one element per each beam layer in the transverse direction was utilized. The total number of unknowns in the model was about of 26,000. Time increments used in the temporal discretization are automatically chosen by ABAQUS/Explicit on the basis of a maximum natural frequency in the underlying FE model. For the elaborated model, the time increments were approximately of 1.5×10^{-6} s and their total number was about of one million in 2 s of the analysis time.

The deformed form of the beam at the instant of loading is shown in Fig. 4a just to illustrate its FE model. The dynamic transient analysis accounting for the contact–impact behavior between the delaminated layers and cracked edges is performed with ABAQUS/Explicit implementing the computational algorithms described in Sect. 2.

The transverse displacement time history calculated at a point nearest to the free end of the delaminated beam is converted into the frequency domain data via the spectral analysis by using the fast Fourier transform (FFT) within the Matlab software environment [30]. The comparison of frequency contents of the delaminated beam between the experimental data known in [29] and the results predicted by ABAQUS/Explicit are presented in Fig. 4b. From this plot one can see that the numerical results are in a relatively good compliance with the experimental ones. Thereby, the FE model described in the paper possesses an enough capability to be used for modelling the complex non-linear dynamic behavior of plate-like structures.

Table 1 Material properties of the foam-cored sandwich plate

Components	Elastic constants
Foam core	$E_c = 85$ MPa, $G_c = 30$ MPa, $\rho_c = 52\,\text{kg m}^{-3}$
Face sheet	$E_{xx} = E_{zz} = 19.3$ GPa, $E_{yy} = 3.48$ GPa, $G_{zx} = 7.7$ GPa, $G_{xy} = G_{yz} = 1.65$ GPa, $\rho = 1{,}650\,\text{kg m}^{-3}$

3.2 Plate finite element model

One configuration of a sandwich plate containing a penny-shaped debonded zone is used throughout the numerical predictions in what follows. A simply supported rectangular sandwich plate of length $a = 270$ mm and width $b = 180$ mm consisting of a 50 mm-thick WF51 foam core and 2.4 mm-thick GFRP skins is analyzed. The mechanical properties of constituent materials of the sandwich plate, adopted as in the previous paper [20], are given in Table 1. The friction coefficient is accepted $\mu = 0.1$, that is a lower boundary of the range of friction coefficients for plastic–plastic material combinations. The modal damping ratio equals to 1 % of the critical value. In order to study the influence of debond on the sandwich plate dynamics, a range of radii of the debonded zone (Fig. 1) associated with a ratio of the debonded region's area to the area of sandwich plate plane as 5 10, 15 and 20 % are considered in calculations further.

The debonded sandwich plate is subjected to an impulse concentrated force with the amplitude of

$F_0 = 10$ kN during the time $t_* = 1$ ms applied at the central point of its lower skin. It should be noted that the force amplitude is chosen so that neither geometrical nor material nonlinearities are activated. For this purpose an overall deflection of the sandwich plate and stress states within the both skins and the lightweight core of sandwich plate were examined under the applied external force in preliminary studies, which are not presented in the current paper, but are the same as in [31].

Moreover, before the transient dynamic analysis of the debonded sandwich plate, convergence studies concerning refinement of the FE spatial discretization have previously been performed. Both the solution accuracy and the computational cost were taken into account. The general mesh contained finally one layer of the continuum shell elements for skins and ten layers of the brick elements for the core through the plate thickness for the given sandwich plate. The total number of unknowns in the FE model was about of 80,000. The temporal solution was carried out with time increments approximately of 4×10^{-7} s that gave about 150,000 increments for modelling a transient response in 50 ms.

Time histories of transverse displacements and accelerations, calculated at the central point of the upper skin (point N 1 in Fig. 3a) of the sandwich plate without and with the 10 %-sized debond are compared in Fig. 5. One can see that there are significant differences in both waveforms and signal properties between the time histories of intact and debonded sandwich plates. As resulted from Fig. 5a, the waveform of displacement signal of the debonded plate is more disturbed than that of the intact plate, because the transient dynamics of the debonded sandwich plate is accompanied by intermittent contact between the detached skin and the core. As well, the presence of debond increases the amplitude and period of free decay oscillations for the debonded plate. This result is attributed to decreasing the stiffness of the plate due to debond. Moreover, it can be seen that the amplitude of displacement time history for the debonded plate decays faster with a time progression than that for the intact plate, as shown by comparisons of the trend-lines of displacement signals in Fig. 5a. This fact is an evidence of increasing the internal damping capacity in the debonded plate due to the presence of debond, which introduces additional dissipative mechanisms caused by repeated contacts. Figure 5b shows the comparison between acceleration time histories of the sandwich plate with and without debond. It is clearly seen that the signals are so much different. The amplitude of acceleration time series for the debonded sandwich plate significantly larger than that for the corresponding plate without debond. Thereby, intermittent contact occurring between the detached skin and core contributes considerably into the sandwich plate's transient dynamics.

Next, it is shown that the aforementioned effects caused by the debond increase with enlarging the size of the debonded zone. The time histories of the upper skin's central deflection (point N 1) of the sandwich plate with distinct sizes of the debonded zone are presented in Fig. 6a. One can see that the amplitudes of displacement curves and the values of time lag of free decay oscillations (Fig. 6a) as well as the attenuations of displacement signals (see trend-lines in Fig. 6b) are clearly magnified by the debonded zone size. They increase considerably with increasing the debond.

The logarithmic decrement reflecting a damping capacity of the sandwich plate are calculated for those different sizes of the debonded zone. The results are listed in Table 2. It is obviously seen that even in the case of the smallest debond, the logarithmic decrement for the debonded plate is almost twice that of the corresponding intact plate. The logarithmic decrement increases significantly with increasing the debond size. This means that the dissipation of energy in the sandwich plate increases with enlarging the debonded zone. Thus, this damping parameter is a very sensitive characteristic of the presence of debond within sandwich plates. Such results are consistent with vibrational tests of debonded sandwich structures known in the literature, e.g. [32].

Natural frequencies of the sandwich plates with and without debond are determined from acceleration transient time histories collected at the monitored central point N 1, Fig. 3a. The FFT is applied to the sampled signal in the time domain to represent it as a series of spectral peaks in the frequency domain. The positions of those peaks over the frequency range observed are analyzed that provides the calculation of appropriate resonant frequencies. The power spectra of the debonded sandwich plates with respect to the spectrum of the intact plate are compared in Fig. 8a–d.

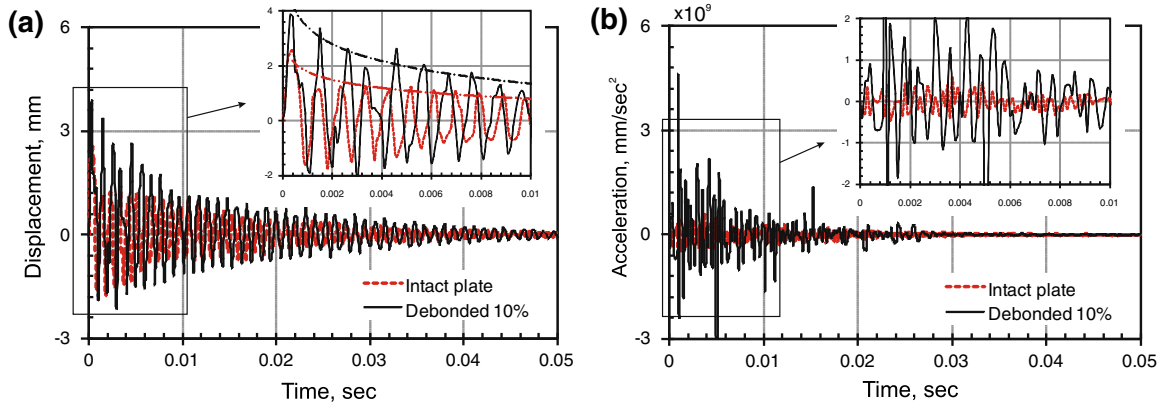

Fig. 5 Transient time histories at the point N 1: **a** displacement; and **b** acceleration

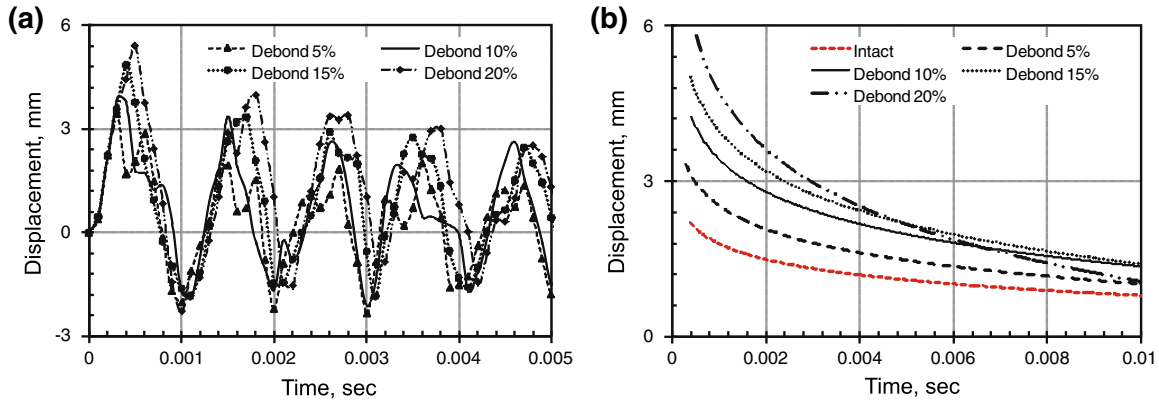

Fig. 6 Transient response for different sizes of debond at the point N 1: **a** displacements; and **b** displacement trend-lines

Table 2 The logarithmic decrement of the intact and debonded sandwich plates

Intact plate	Debonded plate			
	5 %	10 %	15 %	20 %
0.029	0.046	0.104	0.149	0.199

Table 3 Natural frequencies (Hz) of the intact sandwich plate and the sandwich plate with the 10 %-sized debond

Intact	Debonded	Intact	Debonded
1,074.2	957.03	2,832.0	2,675.8
1,562.5	1,308.6	2,968.8	2,792.9
1,757.8	1,406.3	3,144.5	2,910.2
1,953.1	1,621.1	3,261.7	3,007.8
2,187.5	1,953.1	3,378.9	3,281.3
2,285.2	2,109.4	3,496.1	3,359.4
2,578.1	2,382.8	3,750.0	3,593.8
2,675.8	2,500.0	3,808.6	3,785.1

To obtain a better visualization of detected peaks corresponding to actual frequencies, the spectral data are handled by using windowing and smoothing signal-processing techniques. A Hanning window is applied to the resulting spectrum for reducing the spectral leakage occurring in the FFT due to non-periodicity of the predefined time data block. The Savitzky–Golay smoothing based on the least-square fitting of polynomials to the segment of spectral data is used to reduce noise. It is important to notice that this smoothing procedure effectively reduces high-frequency noise to an optimal level of the signal-to-noise ratio while retains the shape of the original signal. A detailed explanation of the spectrum extraction procedure relying on signal-processing techniques is

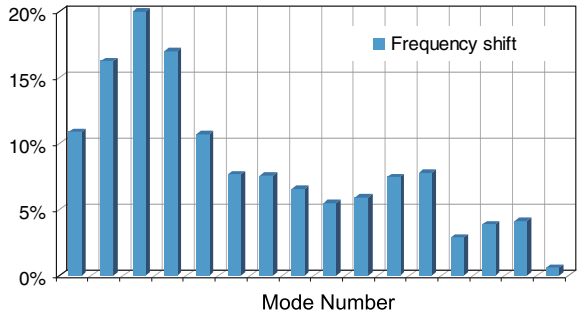

Fig. 7 Relative changes of natural frequencies between the intact plate and the debonded plate with the 10 %-sized debond

beyond the scope of this paper, one can find more information in appropriate books, e.g. [33].

Several natural frequencies extracted by the mentioned above spectrum analysis for the intact plate and the plate with the 10 %-sized debond are listed in Table 3. As seen from Table 3, all the natural frequencies tend to decrease with increasing the number of mode, but this effect does not exhibit a monotonic character. The amount of frequency drop is dependent on the mode of interest, as seen in Fig. 7. More detailed discussions concerning the influence of the debonded zone on natural frequencies and associated mode shapes of sandwich plates can be found in [7, 8].

Analyzing the spectral plots in Fig. 8a–d one can see that the applied load excites predominantly the fundamental mode in all the cases. In doing so, it is seen that the larger is the debonded zone size, the bigger is the reduction in the fundamental frequency in comparison with that of the intact plate. This is due to decreasing the global stiffness as a result of increasing the debond. The wider peaks at the resonant frequencies of the debonded plates indicate higher material damping in them than in the intact plate. The larger is the debond, the wider are the peaks and the less are their amplitudes due to increasing damping with increasing the debond.

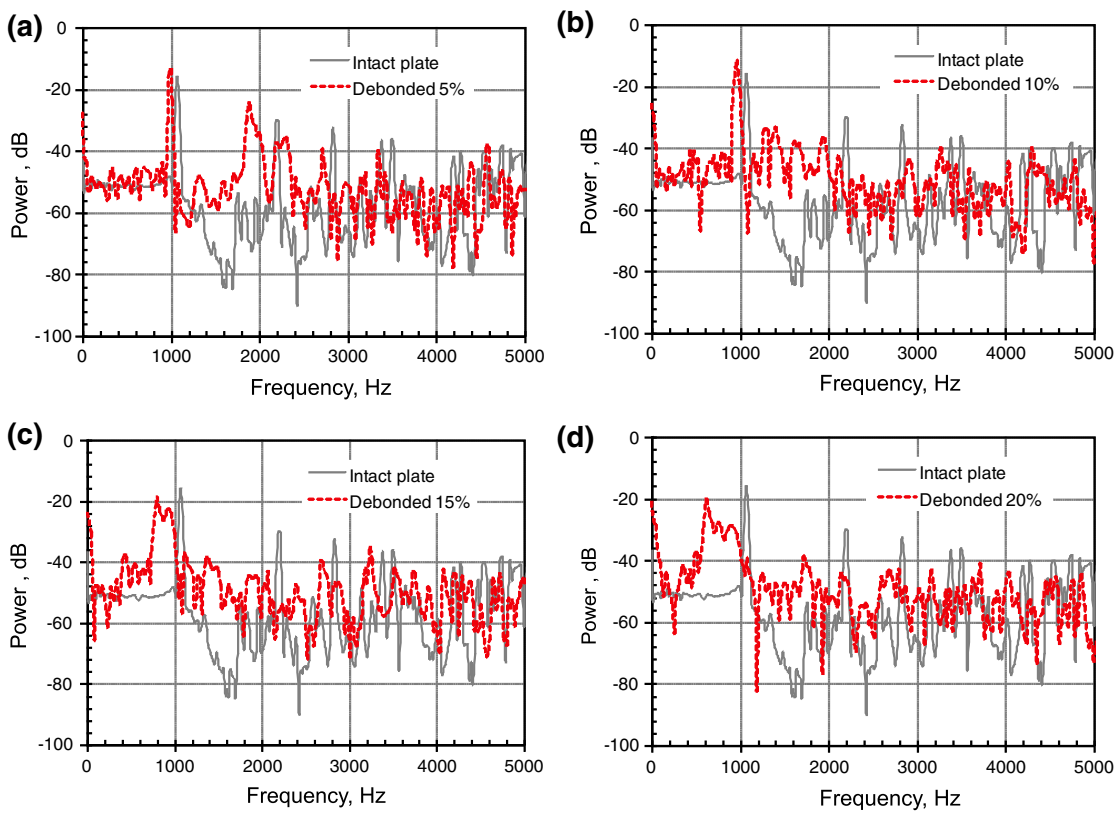

Fig. 8 Power spectra of the sandwich plate with and without debond calculated at the point N 1: **a** 5 %-sized debond; **b** 10 %-sized debond; **c** 15 %-sized debond; and **d** 20 %-sized debond

Another distinctive feature resulting from those frequency signals is the distortion of the shape of peaks around the natural frequencies and the appearance of additional peaks both before and after the fundamental frequency in the frequency spectra of debonded sandwich plates in comparison with the spectrum of the same intact plate, as shown in Fig. 8a–d. This fact is attributed to the intermittent contact behavior between the detached segments in the debonded plates. Those interactions generate additional stress waves that superimpose with waves produced by the external impulse force. In turn, the excited waves spread in the structure in dependence on a state of contact. As a result, wave modulation and frequency mixing can be observed in the frequency response. These results are in qualitative agreement with data reported for dynamics of cracked structures in the literature, e.g. [34, 35]. The behavior indicated by these predictions highlights a high nonlinearity of the debonded plate's transient response.

The enlargement of the debonded zone affects qualitatively and quantitatively the spectrum of the sandwich plate. As shown in Fig. 8a–d, the larger is the debond, the amplitudes of response peaks are bigger before, but smaller after the fundamental frequency. The increasing of the vibration energy at the low frequencies is proportional to the enhancing of friction contact interactions between the detached skin and core for the bigger debond. While the decreasing of the magnitudes of peaks in the high frequency domain is caused by the increasing of the damping capacity of the bigger debond due to clamping and it manifests itself through suppressing the high frequencies. Thereby, the results presented above allow us to conclude that the dynamics of the debonded plate completely depends on a way by which the contact surfaces behave. In this respect the behavior between the detached skin and the remaining part of the plate with 10 %-sized debond is studied in detail further.

Figure 9 compiles the time histories of transverse displacement and velocity of the core and the upper skin calculated at the center of the debonded region (points N 2 and N 3 in Fig. 3b). Tracking the transient motion of the detached fragments in Fig. 9a, one can see that they interact with each other during a defined time interval, after that as the amplitude of vibrations is no longer enough to close the debond, the parts vibrate separately. Referring to Fig. 9b, d, the plots present the transient displacement and velocity time histories, respectively, within the time interval, where interactions between the separated skin and the remaining plate occur. From Fig. 9b it can be seen that at each vibration cycle the distinct phases of motion of the contacting parts such as sudden impact (clamping), permanent contact and separated motion (free flight) can clearly be distinguished. Every contact–impact event is generally characterized by an energy trade-off between the contacting parts and, as a consequence, sharp changes in relative velocities of these parts take place, as shown in Fig. 9d, whereas their relative displacements are less disturbed due to thereof, Fig. 9b. During permanent contact between the detached surfaces, the normal component of their velocities are the same, and the tangential ones can be directed oppositely if sliding of the contacting points with respect to each other occurs. One can notice from Fig. 9a that as the time progresses the duration of permanent contact decreases, and motion with impact-like contacts between the interacting skin and core mainly exists up to ceasing the interactions between them. The above mentioned behavior of the contact–impact motion has also been demonstrated as far as impact oscillators are concerned, e.g. in [36] and presented as results of experimental tests and FEM predictions with beam elements for a delaminated beam in [37].

To separate accurately phases with and without contact between the detached skin and the remaining plate at the monitored central points N 2 and N 3 during vibrations, variations with time of normal and tangential contact forces with respect to the central deflection time histories of these two parts depicted by subtle lines are presented in Fig. 10a, b, respectively. It can be seen that the normal contact forces are essentially bigger than the shear ones at each contact event. Hence, one can conclude that the contacting surfaces interact with each other mainly in the normal direction, however, due to rotation and lateral movement of the thinner detached skin sliding may occur too. These two interaction mechanisms act simultaneously in most of the motion cycles, thus permanent contact, which can be even very short-term, follows impact in most cases. Also Fig. 10a, b show that the contact forces increase first and then gradually reduce with time as the vibrations attenuate. The magnitude of contact forces may seemingly be dependent on different reasons such as inertial forces, local deformed form of the detached fragments and global

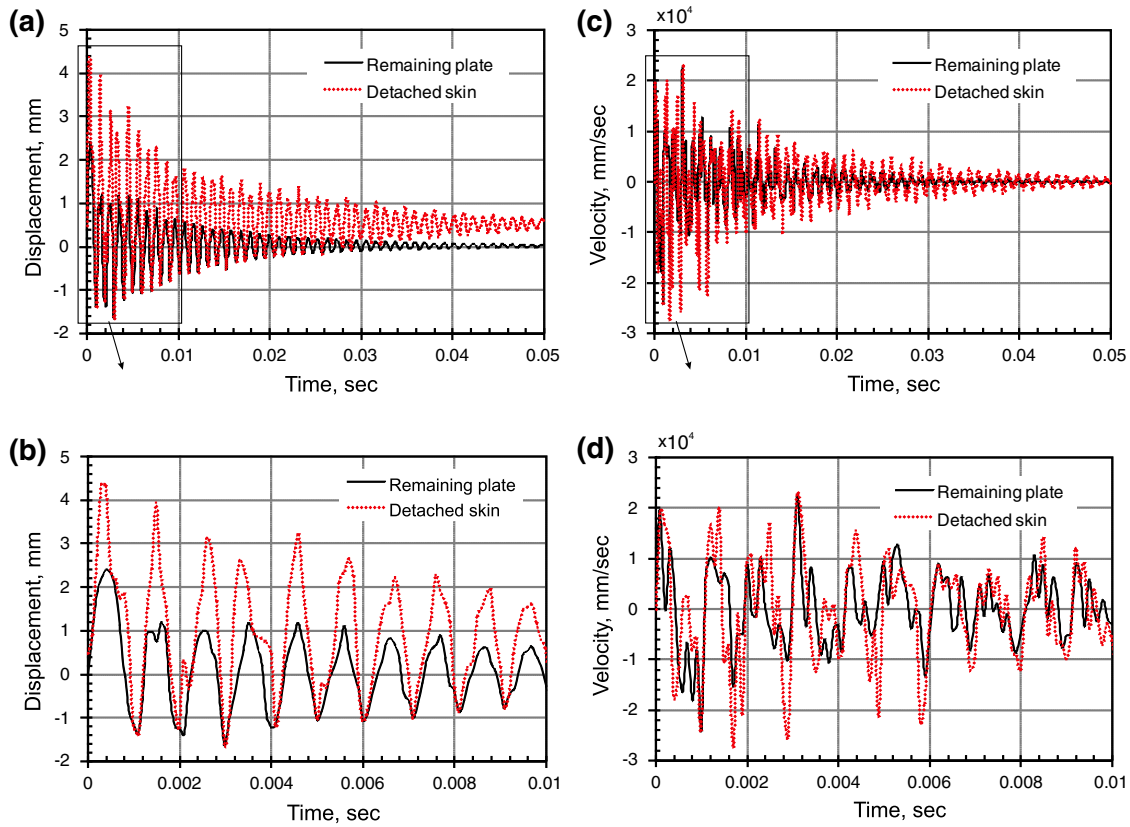

Fig. 9 Time histories of the contacting surfaces at the points N 2 and N 3: **a** displacement during the analysis time; **b** displacement in the time interval $[0; 0.01]$ s; **c** velocity during the analysis time; and **d** velocity in the time interval $[0; 0.01]$ s

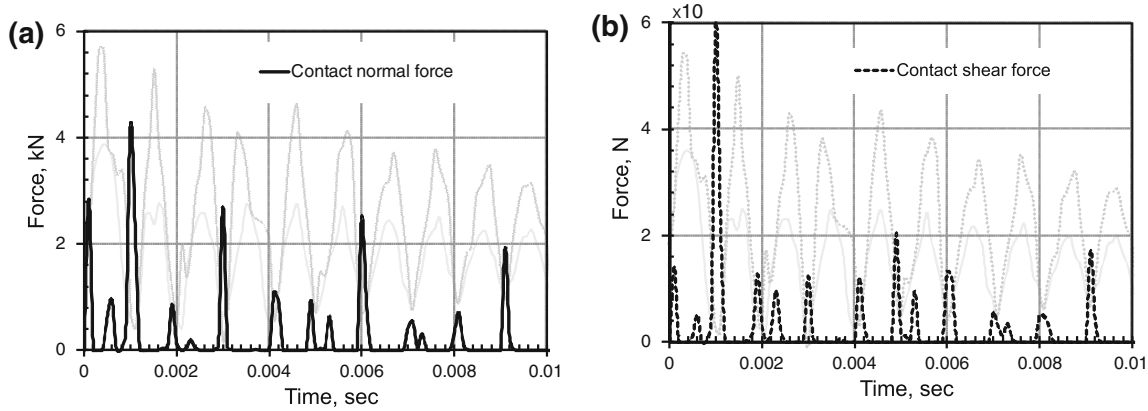

Fig. 10 Time histories of the contacting surfaces at the central point N 2 of the plate with the 10 %-sized debond in the time interval $[0; 0.01]$ s: **a** contact normal force; and **b** contact shear force

deflection pattern of the plate caused by an external load or a combination of all these factors.

The effect of the debond size on the evolution of the contact forces is presented in Fig. 11. The normal and shear contact forces for the smallest and largest debond considered are only presented there. The values of the contact forces for the other cases of the debond size are intermediate between those previous

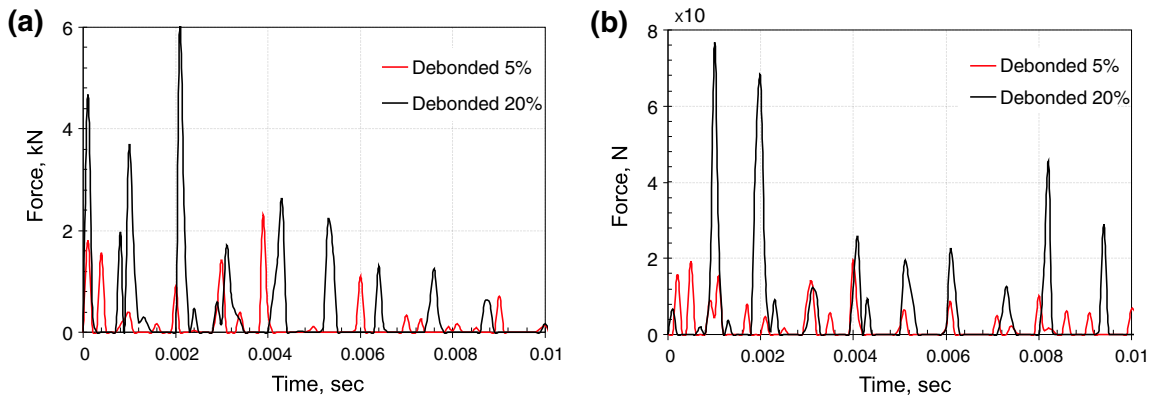

Fig. 11 Time histories of the contact forces, calculated at the central point N 2 depending on the debond size: **a** contact normal force; and **b** contact shear force

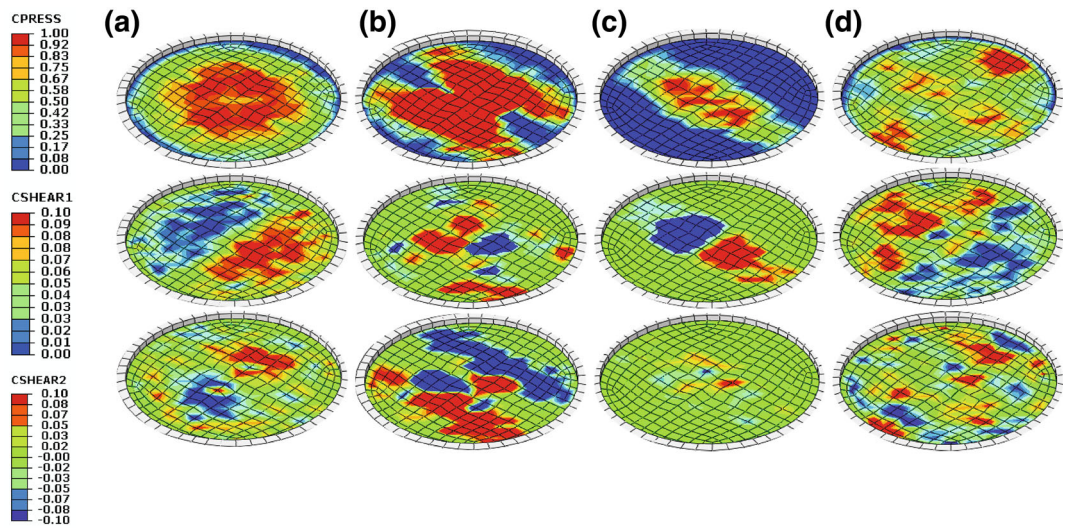

Fig. 12 Distributions of the normal contact traction (*upper row*) and the shear contact stress vectors (*middle and lower rows*) at instants of time: **a** $t = 0.1$ ms; **b** $t = 1$ ms; **c** $t = 4$ ms; and **d** $t = 6$ ms

ones. It can be seen from the figure that with increasing the debonded zone the magnitude of the contact forces increases and the evolution of these forces with time changes. The latter means that the character of contact behavior is changed with variation of the debond size. Thus, the debond size governs the contact behavior completely that in turn influences on the transient response of debonded sandwich plate as pointed out above.

As the debonded sandwich plate is loaded by the impulse force, the plate begins to oscillate. Due to the plate's vibrations the debonded region is passing from closing to opening and vice versa with a continuously developing surface of contact, encompassing a variety of intermediate configurations. Thus, the contact forces arising between the detached skin and the core at each contact point are interconnected within the contact interface. To clearly understand the contact behavior between the detached surfaces, spatial representations of contact force distributions are required. The distributions of both normal and tangential contact stress vectors at certain moments of time for the first six cycles of motion, where contact at the point between the detached segments was noticed in the

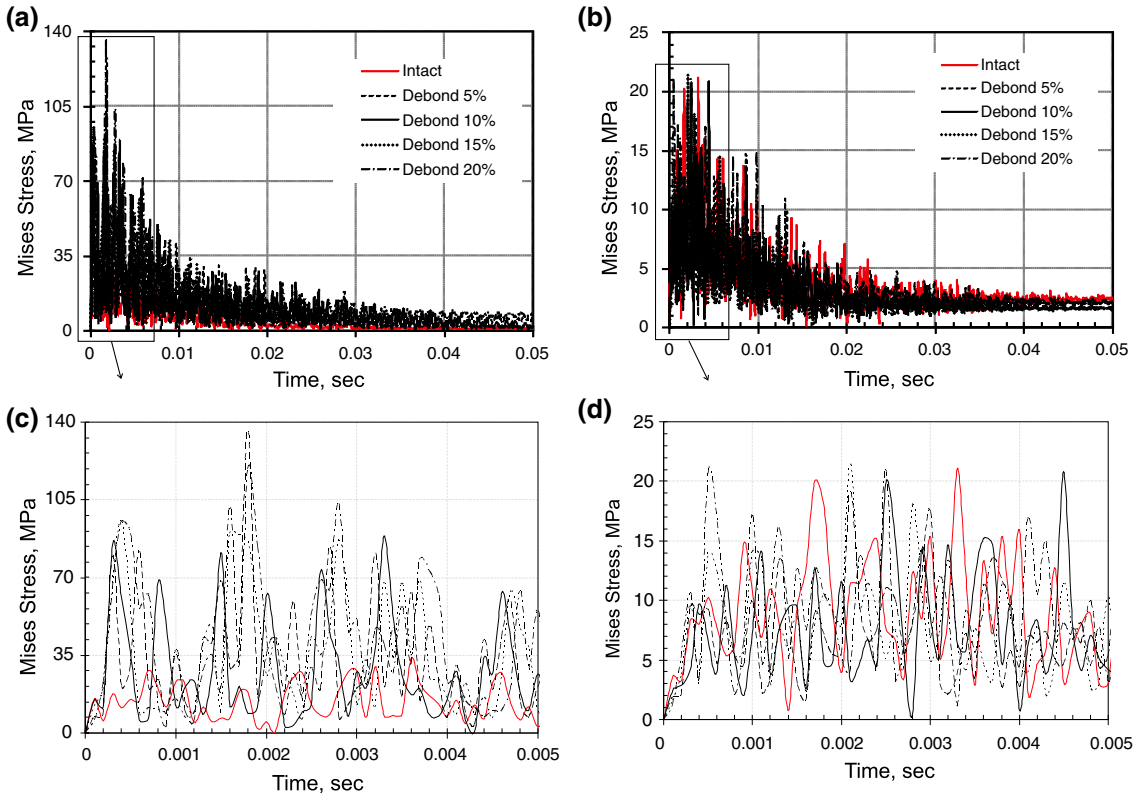

Fig. 13 Time histories of the Mises stress calculated at the point: **a**, **c** inside of the debonded zone (N 4); and **b**, **d** outside of the debonded zone (N 5)

sandwich plate with the 10 %-sized debond (Fig. 10), are displayed in Fig. 12a–d. One can see that variations of the actual normal contact traction due to contact–impact motion of the detached segments change the nature of sliding mechanism that is represented by the appropriate distributions of shear contact stress vectors.

As shown in [20], the contact forces have a considerable influence onto the global dynamic stress state of the debonded sandwich plate. Herewith, stresses are mainly concentrated within the debonded region. To represent the stress concentration occurring within the debonded zone due to the contact interactions, the stresses calculated inside the debonded zone and far away from it are compared for the intact and debonded plates. Figure 13 shows such comparisons between the time histories of Mises stresses computed at the point N 5 which is far away from the debonded zone and at the point N 4 collocating on the boundary of the debonded zone (see Fig. 3a). It is evidently that the Mises stresses of the sandwich plate with and without debond are almost the same at the point far away from the debonded region, but they differ significantly at the internal point of the debonded region. At this point, the stress level of the debonded plate exceeds that of the corresponding intact plate in several times. This effect is more pronounced with enlarging the debond, i.e. the large is the debond, the high stress level takes place within the debonded zone, Fig. 13a, c. While the stress level at the point far away from the debonded region is only slightly affected by the increasing of debond, Fig. 13b, d.

4 Conclusions

Dynamics of the debonded foam-cored sandwich plate subjected to an impulse load is studied using the FEM. The transient dynamic analysis taking into account intermittent contact between the detached segments of the damaged skin-to-core interface is carried out with the ABAQUS/Explicit code. The numerical results

showed that the short-term response of the debonded sandwich plate is considerably affected by the presence of debond. Using the transient time history data predicted, it was identified that contact occurring between the detached skin and the remaining plate, firstly, damps the free decay oscillations making them slower, but faster decaying than those of the intact plate. In doing so, the larger is the debond, the more clearly these effects can be seen. Secondly, the existence of intermittent contact changes the waveforms of the all extracted time histories. Also, in contrast to the intact plate the magnitude of the time signals of the debonded plate is higher. The spectral analysis processed for the time signals of the intact and debonded plates revealed that their frequency contents differ considerably. The reducing of the fundamental frequency and the additional peaks in the both low and high frequency domains are main features of the debonded plate's spectrum in comparison with the spectrum of the intact plate. The shift of the natural frequency and the appearance of the additional frequencies in the spectrum are more significant with increasing the debonded zone. Finally, the dynamic stress state in the debonded plate is evaluated. The link between contact-induced normal and tangential forces within the developing continuous contact surface is found out. As well, a localized character of the contact forces' effects which are mainly restricted by the debonded region is clearly demonstrated by the comparisons between stress histories calculated at the points inside the debonded zone and far away from it. It may be noticed that the finite element model described in this paper can be useful for investigating non-linear transient dynamics of sandwich plates including aspects of damage identification.

Acknowledgments The research leading to these results has received funding from: (1) the European Union Seventh Framework Programme (FP7/2007–2013) FP7-REGPOT-2009-1, project CEMCAST under Grant Agreement No. 245479; (2) Polish Ministry of Science and Higher Education—Grant No. 1471-1/7.PR UE/2010/7; and (3) Ministry of Science and Higher Education within the Statutory Research No. S/20/2013.

References

1. Vinson JR (2005) Plate and panel structures of isotropic, composite and piezoelectric materials. Including sandwich construction. Springer, Dordrecht
2. Carlsson LA, Kardomateas LA (2011) Structural and failure mechanics of sandwich Composites. Springer Science+Business Media B.V., Berlin
3. Hu JS, Hwu Ch (1995) Free vibration of delaminated composite sandwich beams. AIAA J 33:1911–1918
4. Wang Ch, Lam KY, Liu GR (1996) Detection of flaws in sandwich plates. Compos Struct 34:409–418
5. Kim H-Y, Hwang W (2002) Effect of debonding on natural frequencies and frequency response functions on honeycomb sandwich beams. Compos Struct 55:51–62
6. Chakrabarti A, Sheikh AH (2009) Vibration and buckling of sandwich laminates having interfacial imperfections. J Sandw Struct Mater 11:313–328
7. Burlayenko VN, Sadowski T (2010) Influence of skin/core debonding on free vibration behavior of foam and honeycomb cored sandwich plates. Int J Non-Linear Mech 45:959–968
8. Burlayenko VN, Sadowski T (2011) Dynamic behaviour of sandwich plates containing single/multiple debonding. Comput Mater Sci 50:1263–1268
9. Saraswathy B, Mangal L, Kumar RR (2011) Analytical approach for modal characteristics of honeycomb sandwich beams with multiple debond. J Sandw Struct Mater 14:35–54
10. Schwarts-Givli H, Rabinovitch O, Frostig Y (2007) Free vibrations of delminated sandwich panels with a transversely flexible core—a modified Galerkin approach. J Sound Vib 301:253–277
11. Meo M, Vignjevic R, Marengo G (2001) The response of honeycomb sandwich panels under low-velocity impact loading. Int J Mech Sci 47:1301–1325
12. Karagiozova D, Nurick GN, Langdon GS, Yeun SCK, Chi Y, Bartle S (2009) Response of flexible sandwich-type panels to blast loading. Compos Sci Technol 69:754–763
13. Nahvi H, Jabbari M (2005) Crack detection in beams using experimental modal data and finite element model. Int J Mech Sci 47:1477–1497
14. Mustapha S, Ye L, Wang D, Lu Y (2011) Assessment of debonding in sandwich CF/EP composite beams using A0 Lamb wave at low frequency. Compos Struct 93:483–491
15. Ju F, Lee HP, Lee KH (1994) Dynamic responses of delaminated composite beams with intermittent contact in delaminated segments. Compos Eng 4:1211–1224
16. Kwon YW, Lannamann DL (2002) Dynamic numerical modeling and simulation of interfacial cracks in sandwich structures for damage detection. J Sandw Struct Mater 4:175–199
17. Ghoshal A, Kim HS, Chattopadhyay A, Prosser WH (2005) Effect of delamination on transient history of smart composite plates. Finite Elem Anal Des 41:850–874
18. Müller I, Konyukhov A, Vielsack P, Schweizerhof K (2005) Parameter estimation for finite element analyses of stationary oscillations of a vibro-impacting system. Eng Struct 27:191–201
19. Burlayenko VN, Sadowski T (2012) A numerical study of the dynamic response of sandwich plates initially damaged by low velocity impact. Comput Mater Sci 52:212–216
20. Burlayenko VN, Sadowski T (2012) Finite element nonlinear dynamic analysis of sandwich plates with partially detached facesheet and core. Finite Elem Anal Des 62:49–64
21. Laursen TA (2002) Computational contact and impact mechanics: fundamentals of modeling interfacial phenomena in nonlinear finite element analysis. Springer, Berlin

22. Wriggers P (2006) Computational contact mechanics. Springer, Berlin
23. Song J-H, Belytschko T (2009) Cracking node method for dynamic fracture with finite elements. Int J Numer Methods Eng 77:360–385
24. Zozulya VV (2011) Variational formulation and nonsmooth optimization algorithms in elastodynamic contact problems for cracked body. Comput Methods Appl Eng 200:525–539
25. Belytschko T, Liu WK, Moran B (2002) Nonlinear finite elements for continua and structures. Wiley, New York
26. Petyt M (2010) Introduction to finite element vibration analysis. Cambridge University Press, New York
27. Taylor LM, Flanagan DP (1989) PRONTO 3D a three-dimensional transient solid dynamics program. Sandia National Laboratories, Albuquerque
28. ABAQUS (2009) User manual version 6.9EF-1. Dassault Systèmes Simulia Corp., Providence
29. Prime MB, Shevitz DW (1995) Linear and nonlinear methods for detecting cracks in beams. In: Proceedings of the 15th international modal analysis conference, pp 1437–1443
30. MATLAB 7.9 (2009) The MathWorks Inc., Natick
31. Burlayenko VN, Sadowski T (2011) Dynamic analysis of debonded sandwich plates with flexible core numerical aspects and simulation. Adv Struct Mater 15:415–440
32. Baba BO, Thoppul S (2009) Experimental evaluation of the vibration behavior of flat and curved sandwich composite beams with face/core debond. Compos Struct 91:110–119
33. Koopmans LH (1995) The spectral analysis of time series. Academic Press, California
34. Korshak BA, Solodov IY, Ballad EM (2002) DC effects, sub-harmonics, stochasticity and "memory" for contact acoustic non-linearity. Ultrasonics 4:707–713
35. Caddemi S, Caliò I, Marletta M (2010) The non-linear dynamic response of the Euler–Bernoulli beam with an arbitrary number of switching cracks. Int J Non-Linear Mech 45:714–726
36. Foong C-H, Wiercigroch M, Pavlovskaia E, Deans WF (2007) Nonlinear vibrations caused by fatigue. J Sound Vib 303:58–77
37. Müller I (2007) Clapping in delaminated sandwich-beams due to forced oscillations. Comput Mech 39:113–126